



Quantification of the contribution of the Beauce groundwater aquifer to the discharge of the Loire River using thermal infrared satellite imaging

E. Lalot¹, F. Curie¹, V. Wawrzyniak², F. Baratelli³, S. Schomburgk⁴, N. Flipo³, H. Piegay², and F. Moatar¹

¹Laboratoire GEHCO, UFR sciences et techniques, Université François Rabelais, Tours, France

²Plateforme ISIG, CNRS – UMR 5600 EVS, Ecole Normale Supérieure de Lyon, Université de Lyon, Lyon, France

³Centre de Géosciences – Systèmes hydrologiques et Réservoirs, Mines ParisTech, Fontainebleau, France

⁴Dir. Eau Environnement et Ecotechnologies, Bureau de Recherches Géologiques et Minières (BRGM), Orléans, France

Correspondence to: E. Lalot (eric.lalot@gmail.com)

Received: 19 December 2014 – Published in Hydrol. Earth Syst. Sci. Discuss.: 16 February 2015

Revised: 14 August 2015 – Accepted: 8 September 2015 – Published: 9 November 2015

Abstract. Seven Landsat thermal infrared (TIR) images taken over the period 2000–2010 were used to establish longitudinal temperature profiles of the middle Loire River where it flows above the Beauce aquifer. The groundwater discharge along the river course was quantified for each identified groundwater catchment area using a heat budget based on temperature variations of the Loire River estimated from the TIR images. The results showed that 75 % of the temperature differences, between in situ observations and TIR image-based estimations, remained within the $\pm 1^\circ\text{C}$ interval. The main discharge area of the Beauce aquifer into the Loire River was located between river kilometers 630 and 650, where there was a temperature drop of $1\text{--}1.5^\circ\text{C}$ in the summer and a rise of 0.5°C in winter. According to the heat budgets, groundwater discharge was higher during the winter period ($13.5\text{ m}^3\text{ s}^{-1}$) than during the summer period ($5.3\text{ m}^3\text{ s}^{-1}$). These findings are in line with the results of both a groundwater budget and a process-based distributed hydrogeological model. Groundwater input was also found to be higher during the Loire's flow recession periods.

temperature and groundwater discharge (Webb and Zhang, 1997, 1999; Hannah et al., 2004). However, quantifying the respective influence of these factors is often difficult, since temperature profiles of the river course have first to be established.

Since the late 1990s, thermal infrared (TIR) images have been used to determine river water temperature along sections ranging from tens to hundreds of kilometers (Torgersen et al., 2001; Handcock et al., 2006, 2012). Until now, these images of watercourses have mainly been used (i) to identify cold refuges for fish in the summer (Belknap and Naiman, 1998; Torgersen et al., 1999; Tonolla et al., 2010; Monk et al., 2013); (ii) to study the thermal variability of rivers or alluvial floodplains and locate areas of similar thermal characteristics (Smikrud et al., 2008; Tonolla et al., 2010; Wawrzyniak et al., 2012, 2013, Fullerton et al., 2015); and (iii) to validate river temperature models (Boyd and Kasper, 2003; Cristea and Burges, 2009).

Most of these studies have been based on airborne TIR images, while studies based on TIR satellite images are scarce, mainly due to their poor spatial resolution. In the case of the Landsat 7 satellite, 1 pixel of the TIR image represents $60\text{ m} \times 60\text{ m}$ on the ground. Therefore, only a few large river courses can be studied using TIR satellite images, as it is usually considered that river width must exceed 3 image pixels to provide an accurate estimation of water temperature (Handcock et al., 2006; Wawrzyniak et al., 2012). Three pixels is usually considered to be the absolute minimum (Torgersen et

1 Introduction

Water temperature is a key factor for aquatic fauna (Ward, 1992; Caissie, 2006). For instance, it controls oxygen dissolution, essential for aquatic organisms. River temperature is controlled by many factors such as net solar radiation, air

al., 2001). However, the advantage of Landsat satellite images over airborne images is that they are freely available at different dates, providing archives to explore inter-annual or seasonal patterns. As the surface area covered by a single satellite image would require a long time to be covered by air, longitudinal thermal profiles derived from TIR satellite images also show less bias due to change in water temperature during sampling time.

Groundwater discharge has already been shown to have a significant influence on surface water temperature (Hannah et al., 2004; Webb and Zhang, 1997, 1999); however, this influence has seldom been studied using TIR images (Loheide and Gorelick, 2006; Burkholder et al., 2007; Wang et al., 2008; Danielescu et al., 2009; Mallast et al., 2014). Only one paper describes a test to quantify the groundwater discharge in a small stream, based on the longitudinal temperature profile established from airborne TIR images (Loheide and Gorelick, 2006). To our knowledge, groundwater discharge into rivers has never been observed or quantified using satellite TIR images.

Locating groundwater discharge areas is crucial to assess the vulnerability of aquatic fauna, as these locations can act as sheltered areas (Belknap and Naiman, 1998). Understanding water temperature variations along the middle Loire River, where several nuclear power plants are located, is an operational issue for Electricité De France (EDF). For example, between the nuclear power plants of Dampierre and Saint-Laurent-des-Eaux, the Loire River temperature has been shown to be influenced by the groundwater discharge from the Beauce aquifer and the Val d'Orléans hydrogeological system (Alberic and Lepiller, 1998; Alberic, 2004; Moatar and Gailhard, 2006). The average discharge of the Beauce aquifer was previously quantified using hydrogeological numerical modeling (Monteil, 2011; Flipo et al., 2012) and was found to have an inter-annual average of approximately $10 \text{ m}^3 \text{ s}^{-1}$. However, until now, field measurement data have not been used to accurately locate or quantify the groundwater discharge.

The main aims of this study were therefore to test the ability of thermal infrared images from the Landsat satellite (i) to accurately determine water temperature in a river with a width of less than 180 m; (ii) to characterize the longitudinal and temporal variations of temperature along a 135 km section of the middle Loire River overlying the Beauce aquifer between Dampierre and Blois; and (iii) to locate and quantify the contribution of the Beauce aquifer groundwater discharge into the Loire River.

2 Study area

The study site was the Loire River between Gien and Blois (a 135 km reach), which overlies the Beauce aquifer (Fig. 1). The catchment area of the Loire at Gien is $35\,000 \text{ km}^2$ and

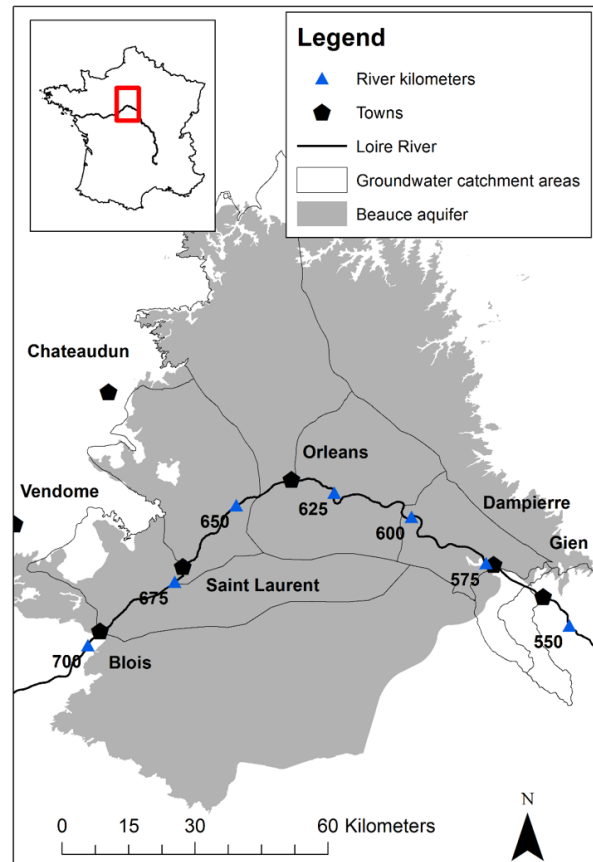


Figure 1. Map of the study area. The delineation of the Beauce aquifer comes from the BDLISA database from the Bureau de Recherches Géologiques et Minières (BRGM).

the river slope is 0.4 m km^{-1} in the studied section (Latapie et al., 2014).

The river flow rate is measured daily in Gien, Orléans and Blois, respectively, at river kilometers 560, 635 and 695 (Banque HYDRO: www.hydro.eaufrance.fr). Over the 1964–2011 period, in Orléans the average flow rate was $345 \text{ m}^3 \text{ s}^{-1}$, and the average flow rates in August and January were 95 and $553 \text{ m}^3 \text{ s}^{-1}$, respectively.

The width of the wet section of the middle Loire River ranges between 200 and 450 m (Latapie et al., 2014). However, during low flow periods (i.e., below $100 \text{ m}^3 \text{ s}^{-1}$), the Loire River forms several branches locally and the main branch width can be as low as 50 m. During these periods, the average river depth is about 1 m in the studied reach. Along the Loire River, the main natural and artificial weirs are located at river kilometers 571, 603, 635, 661, and 670, where the water level shows a drop of just over 1 m during low flow periods.

The climate of the study area is temperate. The mean annual air temperature in Orléans is 11°C . The cold season lasts from mid-November to early March, with an average air temperature of 4.0°C (data from Météo France at Or-

léans station for the period 1961–1990). The warm season lasts from late May to early September, with an average air temperature of 17.2 °C.

The water temperature of the Loire River is influenced by several factors: (i) atmospheric heat fluxes from direct solar radiation, diffuse solar radiation, latent heat exchange, conduction and water-emitted radiation; (ii) groundwater discharge from the Beauce aquifer and Val d'Orléans hydrosystem (Alberic, 2004; Gutierrez and Binet, 2010); (iii) warm water originating from the cooling systems of the nuclear power plants of Dampierre and Saint-Laurent-des-Eaux (average discharge of $2 \text{ m}^3 \text{ s}^{-1}$ from nuclear reactors). However, the nuclear power plants only have a slight influence on the temperature of the river, as the cooling towers remove much of the heat. The median temperature rise between the upstream and downstream sections of the nuclear power plants is 0.1 °C with a 90th percentile of 0.3 °C (Bustillo et al., 2014). The greatest increase in river temperature due to the power plants is observed in winter, during low flow periods (< 1 °C). (iv) In-flows from the tributaries. The catchment area of the Loire River between Gien and Blois is around 5600 km² (a 16 % increase in the catchment area over the 135 km reach). The influence of the tributaries on the river temperature is considered negligible in this section, since the water temperature of the tributaries is usually close to that of the Loire itself (Moatar and Gailhard, 2006) and the flow rates of the tributaries are low (less than $1 \text{ m}^3 \text{ s}^{-1}$). However, in this section, the main tributary of the Loire is the Loiret, which drains water originating from both the Beauce aquifer and the Loire (Alberic, 2004; Binet et al., 2011) and is very short (6 km). The influence of the Loiret River can therefore be included with that of the Beauce aquifer.

3 Material and methods

3.1 Data

Seven satellite images from the Landsat 7 ETM+, presenting cloud cover under 10 %, were extracted from the period 1999–2010 (<http://earthexplorer.usgs.gov/>) (Table 1). Five images were available in the warm season and two in the cold season. They were taken at 12:30 LT in summer and 11:30 LT in winter. Each image covered the entire course of the Loire River between Gien and Blois.

Water temperatures of the Loire River are monitored by EDF upstream of the nuclear power plant of Dampierre (river kilometer 571) and Saint-Laurent-des-Eaux (river kilometer 670) on an hourly basis. The average daily water temperature observed, on the days when the images were taken, was 5.2 °C in the cold season and 23.7 °C in the warm season.

River flow rates measured in Orléans, on the days the images were taken, were between 61 and $478 \text{ m}^3 \text{ s}^{-1}$. On six out of the seven dates, the Loire River discharge/flow rate was lower than the mean annual flow ($345 \text{ m}^3 \text{ s}^{-1}$).

3.2 Extraction of the longitudinal temperature profiles of the Loire River

The first step was to locate pixels corresponding to water only. To this end, a threshold based on the TM 8 band of the Landsat images (0.52–0.9 μm; USGS, 2013) was used and only values below the threshold were kept. The aerial images in the visible range from the Ortho database, of the Institut National de l'information Géographique et forestière (IGN), were used to set the threshold value for each image by comparing the TM 8 band to the Loire watercourse in known locations and where it did not alter with time. The Carthage database from the IGN, which maps all the French watercourses as lines, enabled the water pixels belonging to the Loire River to be separated from those belonging to other water bodies. As shade resulting from the clouds merges with the water pixel, it was removed manually using the same TM 8 band. The main advantage of using the TM 8 band to detect water is that its spatial resolution (15 m) is much higher than that of the TM 61 band (60 m resolution, sub-sampled at 30 m; 10.4–12.5 μm), which is used to estimate water temperature.

A previous study (Handcock et al., 2006) demonstrated that river temperatures should be estimated using only pure water pixels (i.e., separated from the river banks by at least another water pixel). However, in the case of the middle Loire River, pure water pixels could not be found along the entire river course, especially at low flow rates. Therefore, all water pixels were kept. Pixels composed of land and water were considered as land pixels.

In order to detect the water pixels from the TM 61 infrared band, a neighborhood analysis was therefore conducted, based on the water and land pixels already identified from the TM 8 band. Only pixels from the TM 61 band situated further than 60 m away from the already identified land pixels (using the TM 8 band) were kept. To detect pure water pixels, a 120 m buffer zone was used.

The temperature was then calculated for these identified Loire pixels from the radiance values extracted from the TM 61 band of the Landsat images using Planck's law (Chander et al., 2009). A value of 0.98 was used for water emissivity. No atmospheric correction was taken into account, since the study area was included in a single LANDSAT image and atmospheric conditions were homogeneous within the study area (with less than 10 % of cloud cover). Finally, temperature values for these pixels were projected orthogonally on the longitudinal profile of the Loire extracted from the Carthage database. The average temperature for 200 m long sections was then calculated. A distance of 200 m was chosen to be similar to the width of the Loire River. After this, a moving average for 10 consecutive temperature values along the watercourse (2 km) was calculated to smooth the temperature profile.

The temperature profiles extracted from the TIR images were then used for two different purposes: (i) the accuracy

Table 1. Loire River temperature, air temperature and river flow rate at the date and time satellite images were taken.

	Date	Daily river flow in Orléans (m ³ s ⁻¹)	Hourly mean water temperature		Hourly air temperature
			in Dampierre (°C)	in Saint-Laurent-des-Eaux (°C)	in Orléans (°C)
Winter	15 Nov 2001	182	5.2	5.8	5.6
	22 Feb 2003	478	4.2	5.5	12.7
Summer	29 May 2003	89	22.8	20.1	25.5
	19 Jul 2010	112	23.4	23.1	28.3
	20 Aug 2010	78	21.8	20.9	28.3
	24 Aug 2000	83	24.0	22.5	30.4
	29 Jul 2002	61	28.3	26.0	32.5

and uncertainty of the temperatures estimated from the TIR images were tested by comparing them with the hourly in situ measurements conducted by EDF at Dampierre and Saint-Laurent-des-Eaux; (ii) a heat budget method, based on the temperature estimated from the TIR images, was used along successive sections of the Loire River to quantify the groundwater discharge for each section. The results were then compared with the groundwater discharge calculated using a deterministic process-based groundwater model applied over the whole Loire River basin. Calculated groundwater discharge estimations were compared over successive groundwater catchment areas along the Loire River.

3.3 Groundwater discharge estimation based on heat budget

The middle Loire River was divided into 11 sections, so that for each section there was only one groundwater catchment area on each side of the river. The groundwater catchment areas were delineated using available piezometric maps, or elevation data (surface water catchment area) when the maps were missing. A description of the method can be found in Schomburgk et al. (2012). The first section begins at river kilometer 560, where the flow rate is measured (Gien). The groundwater discharge was estimated on each section using a heat budget based on the temperatures derived from the TIR images.

The heat budget equilibrium can be written as (Moatar and Gailhard, 2006)

$$\rho C Q_{i-1} T_{i-1} + F_{\text{net}} S + \rho C Q_{\text{gw}} T_{\text{gw}} = \rho C Q_i T_i, \quad (1)$$

$$Q_{i-1} + Q_{\text{gw}} = Q_i. \quad (2)$$

The groundwater discharge in the section (Q_{gw}) can be deduced:

$$\frac{\rho C Q_{i-1} (T_{i-1} - T_i) + F_{\text{net}} S}{\rho C (T_i - T_{\text{gw}})} = Q_{\text{gw}}. \quad (3)$$

Q_{i-1} (m³ s⁻¹) is the upstream flow rate of the section at temperature T_{i-1} (°C), and Q_i (m³ s⁻¹) is the downstream

flow rate of the section at temperature T_i (°C). Q_{gw} (m³ s⁻¹) is the groundwater flow rate at temperature T_{gw} (°C). For each section, the flow entering the section is equal to the flow entering the previous section plus the groundwater discharge estimated over the previous section (only taken into account if the estimated discharge was positive). The groundwater temperature was considered to be 12.6 °C in summer and 12.1 °C in winter, based on 292 measurements from the ADES database (www.ad.es.eaufrance.fr) conducted in the vicinity of the Loire River, over the 1991–2011 period. Over 80 % of the temperature measurements were included in the interval mean plus or minus 1.4 °C. F_{net} (W m⁻²) stands for the atmospheric heat flux and S (m²) is the surface area covered by the Loire River on the section. S was estimated for each section by adding the surface areas of all the water pixels identified on the satellite images from the TM 61 band. This value was therefore somewhat underestimated, as image pixels composed of both water and land were not included. ρ is the water density (kg m⁻³) and C (J kg⁻¹ K⁻¹) is the specific heat of water.

The heat flux (F_{net}) between the Loire River and the atmosphere was estimated as follows (Salencon and Thébaud, 1997; Chapra, 1997; Table 2):

$$F_{\text{net}} = RA + RS - RE - CV - CE, \quad (4)$$

where RA is atmospheric radiation, RS solar radiation, RE emitted radiation, CV the conduction and CE the condensation/evaporation.

The atmospheric parameters extracted from the SAFRAN (Système d'Analyse Fournissant des Renseignements Adaptés à la Nivologie) database from Météo France (Quintana-Segui et al., 2008) were averaged along the successive Loire River sections. All the atmospheric factors were averaged over the 24 h period preceding the acquisition of the infrared image. This choice is questionable as the water temperature in the Loire River may be influenced by changes in atmospheric factors over a longer time period. However, the travel time of water between Gien and Blois was between 1 and 1.5 days on the dates when the images were taken. Atmo-

Table 2. Details of the atmospheric heat flux calculations.

Solar radiation	RS estimated from the SAFRAN database	Details
Atmospheric radiation	$RA = \sigma (T_a + 273.15)^4 (A + 0.031\sqrt{e_a})(1 - R_L)$	T_a (°C) is the air temperature estimated from the SAFRAN database from Météo France, $\sigma = 4.9 \times 10^{-3} \text{ J m}^{-2} \text{ d}^{-1} \text{ K}^{-4}$ is the Stefan–Boltzman constant, $A = 0.6$ $R_L = 0.03$ are attenuation and reflection coefficients, $e_a = 1.22Q_a$ is the air vapor pressure, and Q_a in g kg^{-1} is the specific humidity of air estimated from the SAFRAN database.
Emitted radiation	$RE = \varepsilon \sigma (T_w + 273.15)^4$	$\varepsilon = 0.98$ is the water emissivity, and T_w (°C) is the mean water temperature on the section estimated from the longitudinal temperature profiles.
Conduction	$CV = \rho_a C_a e(V) (T_w - T_a)$	$\rho_a = 1.293 \left(\frac{273.15}{T}\right)^3$ air density in kg m^{-3} is the function of air temperature T (K) estimated from the SAFRAN database, $C_a = 1002 \text{ J kg}^{-1} \text{ C}^{-1}$ is the specific heat of air, $e(V) = 0.0025*(1 + V_2)$ is the function of the wind 2 m above the ground V_2 ($\text{m}^3 \text{ s}^{-1}$), and $V_2 = V_{10} \left(\frac{2}{10}\right)^{0.11}$ is used to estimate the wind 2 m above the ground as a function of the wind 10 m above the ground, itself estimated from the SAFRAN database.
Condensation/evaporation	$CE = L(T_w) \rho_a e(V) (Q_w - Q_a)$	$L(T_w) = (2500.9 - 2.365T_w) 10^3 \text{ J kg}^{-1}$ is the latent evaporation heat $Q_w = \frac{4.596 \cdot e^{237.3/T_w}}{1.22}$, and Q_a in g kg^{-1} is the specific humidity of saturated air at the water temperature.

spheric parameters were therefore not integrated over a period exceeding a day.

As the Loire River course is wide, no shading from the alluvial forest was taken into account.

3.4 Groundwater discharge estimation based on groundwater modeling

The Eau-Dyssée model was used to determine the groundwater discharge along the Loire River. Eau-Dyssée is an integrated, distributed, process-based model that allows the simulation of the main components of the water cycle in a hydrosystem. Detailed descriptions of the model can be found in Flipo et al. (2012) and Saleh et al. (2011). This model has been applied to basins of different scales and hydrogeological settings, e.g., the Oise basin (4000 km²; Saleh et al., 2011), the Rhône basin (86 500 km²; Habets et al., 1999; Etchevers et al., 2001), the Seine basin (65 000 km²; Ledoux et al., 2007; Pryet et al., 2015) and the Loire basin (120 000 km²; Monteil, 2011).

Eau-Dyssée divides a hydrosystem conceptually into three interacting compartments: a surface, an unsaturated zone and a saturated zone. Specifically, the model couples different modules, which simulate the mass balance of surface water, the runoff, the river flow rate, the fluctuations of in-stream water levels, and the flow rate in the unsaturated and saturated zones.

The water flux q_{sa} ($\text{m}^3 \text{ s}^{-1}$) at the stream–aquifer interface is computed using a conductance model; i.e., it is proportional to the difference between the piezometric head, h_g (m) and the in-stream water level, h_r (m), i.e.,

$$q_{sa} = k_{riv} (h_g - h_r), \tag{5}$$

where the proportionality constant k_{riv} ($\text{m}^2 \text{ s}^{-1}$) is the conductance of the stream–aquifer interface. Rushton (2007)

showed that the main factor controlling this coefficient is the horizontal hydraulic conductivity k_H (m s^{-1}) of the underlying aquifer.

$$k_{riv} = f k_H L, \tag{6}$$

where f (–) is an adjustable correction factor, generally ranging between 0.9 and 1.2 (Rushton, 2007), and L (m) is the length of the river in the aquifer mesh.

Eau-Dyssée was applied to the Loire basin by Monteil (2011). In-stream water levels were assumed to be constant. This work has been improved by simulating the time variability of in-stream water levels with a Manning–Strickler approach (Chow, 1959). Under the assumptions that the river section is rectangular and that its width is much greater than its depth, h_r is given by

$$h_r = b + \left(\frac{Q}{\alpha \kappa W S^{1/2}} \right)^{5/3}, \tag{7}$$

where b (m) is the riverbed elevation, Q ($\text{m}^3 \text{ s}^{-1}$) is the discharge, $\alpha = 1 \text{ m}^{1/3} \text{ s}^{-1}$, κ (–) is the Strickler coefficient, W (m) is the river width, and S (–) is the slope of the riverbed.

Details on the input data and model calibration can be found in Monteil (2011). The morphological parameters of the Loire River (river width and riverbed elevation and slope) were estimated from several cross sections surveyed with an average spacing of 1.6 km (Latapie et al., 2014). Strickler’s coefficient was calibrated against observed hydrographs at six stations along the Loire River, three of which are located on the Beauce aquifer.

The stream–aquifer exchanges were simulated in the period 1996–2013 at a daily time step for the river network at a 1 km resolution. Groundwater discharge was then calculated for the 11 Loire River sections selected for the heat budget.

3.5 Uncertainty in groundwater discharge estimation

Equation (3) was used to estimate the uncertainty associated with the groundwater discharge calculated with the heat budget. The absolute uncertainty of the calculated groundwater discharge ΔQ_{gw} can be computed as

$$\begin{aligned} \Delta Q_{\text{gw}} = & \left| \frac{\rho C (T_{i-1} - T_i)}{\rho C (T_i - T_{\text{gw}})} \right| \Delta Q_{i-1} \\ & + \left| \frac{\rho C Q_{i-1}}{\rho C (T_i - T_{\text{gw}})} \right| \Delta (T_{i-1} - T_i) \\ & + \left| \frac{F_{\text{net}}}{\rho C (T_i - T_{\text{gw}})} \right| \Delta S \\ & + \left| \frac{(\rho C Q_{i-1} (T_{i-1} - T_i) + F_{\text{net}} S)^2}{\rho C (T_i - T_{\text{gw}})} \right| \Delta (T_i - T_{\text{gw}}). \quad (8) \end{aligned}$$

ΔQ_{i-1} is the absolute uncertainty in the river flow rate. A 10 % uncertainty in the flow estimation is considered:

$$\Delta Q_{i-1} = 0.1 Q_{i-1}. \quad (9)$$

$\Delta (T_{i-1} - T_i)$ is the absolute uncertainty in the river temperature variations over the corresponding river section. It is computed based on the known spatial variation between Dampierre and Saint-Laurent-des-Eaux of the difference between the temperature estimated from the TIR images and that estimated from in situ measurements. At each date, a difference by river kilometer and then by river section was calculated. The value of this difference was added to T_i (i.e., $T_{i_{\text{new}}}$) to estimate the variation in surface water temperature that could be caused by uncertainties in the measurements: $(T_{i_{\text{new}}} - T_i)$.

$$\Delta (T_{i-1} - T_i) = \left| (T_{i-1} - T_{i_{\text{new}}}) - (T_{i-1} - T_i) \right|. \quad (10)$$

ΔS is the absolute uncertainty in the water surface estimate. It was computed based on the difference between the water surface estimated from the TM 61 band and from the TM 8 band of the Landsat satellite. ΔS was calculated at each date for every study section of the Loire (11 sections).

$\Delta (T_i - T_{\text{gw}})$ is the absolute uncertainty of the difference between the river temperature and the groundwater temperature. It was considered to be equal to 2 °C in order to take into account both groundwater temperature variability and surface water temperature accuracy.

4 Results

4.1 Temperature accuracy and temperature uncertainty

Temperature accuracy is the average difference between the temperature estimated from the TIR images and the temper-

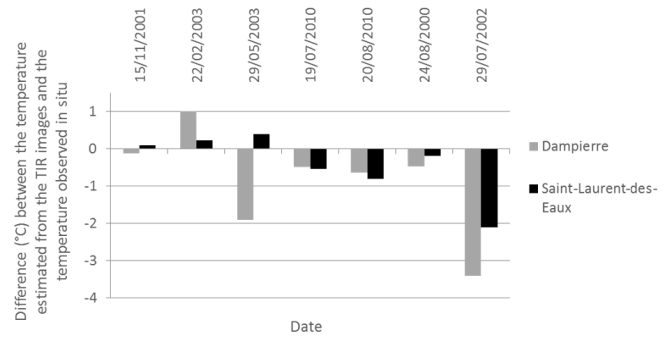


Figure 2. Differences between TIR-derived temperatures extracted from the longitudinal temperature profile and in situ measurements (at the same date and time) for each date and at two different sites (Dampierre and Saint-Laurent-des-Eaux). The dates are classified according to the air temperature at the time when the images were taken (air temperature rose from 15 November 2001 to 29 July 2002).

ature measured in situ (Handcock et al., 2012). The comparison between the in situ and TIR-derived temperatures shows that, on average, the TIR images tend to overestimate the Loire River water temperature in winter (+0.3 °C) and to underestimate it in summer (−1 °C). Over 75 % of the TIR-derived temperatures were between ±1 °C of the temperature measured directly in the river (11 times out of 14; Fig. 2). However, the temperature difference exceeded 1.5 °C on 29 May 2003 and on 29 July 2002 at the Dampierre station and on 29 July 2002 at Saint-Laurent-des-Eaux.

Temperature uncertainty can be linked to the repeatability of the measurement (Handcock et al., 2012). The study of the longitudinal changes of the difference between TIR image-based temperature and in situ measurements may give an idea of the degree of uncertainty (Fig. 2). On average, the variation in temperature difference remained below 0.8 °C over the 100 km reach from Dampierre to Saint-Laurent-des-Eaux, except on 29 July 2002 (1.3 °C) and on 29 May 2003 (2.3 °C). The variation of the temperature difference was between 0.0004 and 0.02 °C km^{−1} (mean of 0.007 °C km^{−1}).

Tests were carried out to assess the influence of the nature of the water pixels (pure or non-pure) on the estimated temperature. For the 200 m long sections of the Loire River where pure water pixels exist, temperature was estimated for both pure and non-pure water pixels. A linear regression was conducted for the temperature estimated with pure water pixels and that estimated with non-pure water pixels. Taking into account the data from all the dates, the slope of the regression line is 1, while it is 0.98 when summer alone is considered and 0.72 for winter alone (Fig. 3a, b). The difference between the temperatures estimated from pure and non-pure water pixels generally remained in the ±0.5 °C interval (over 98 % of the time), which corresponds to the approximate resolution of the satellite sensors. Therefore, taking into account

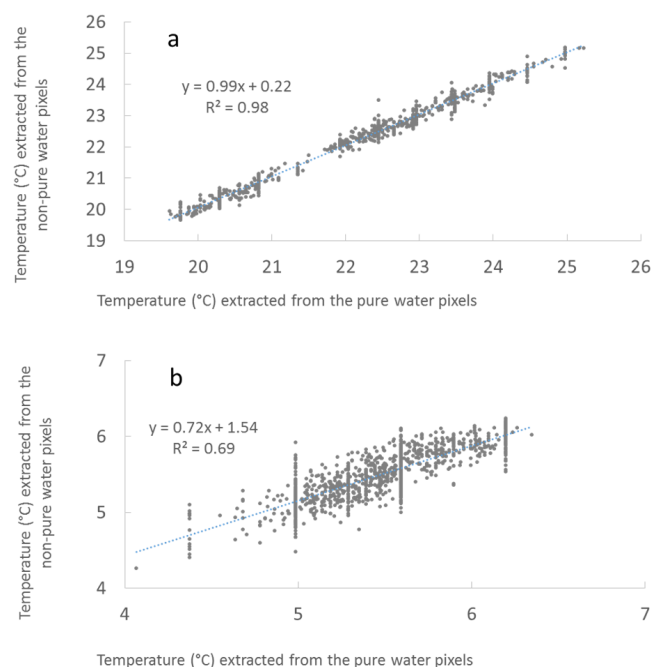


Figure 3. Relationship between the temperatures extracted from the non-pure water pixels and those from the pure water pixels. Temperature values of both pixel types were averaged over the successive 200 m sections where pure water pixels existed. (a) Summer temperatures are represented. (b) Winter temperatures are represented.

non-pure water pixels does not seem to cause a large bias in the case of the Loire River.

However, when the number of water pixels in a 200 m section of the Loire River decreases due to the river being narrower, the standard deviation of the observed temperature increases notably (Table 3). Peak temperature values along the longitudinal temperature profile may therefore appear in places where the main river branch is particularly narrow. This phenomenon is mostly due to the uncertainties inherent in the satellite sensor. Uncertainty can be reduced by averaging and, as the number of pixels considered over a section increases, the uncertainty decreases. The moving average over +2 km that was applied to the data was therefore useful in reducing the uncertainty.

4.2 Longitudinal temperature profiles

Among the seven longitudinal temperature profiles, three main profile types can be observed: two in summer and one in winter (Fig. 4a, b).

In summer, a mean decrease in the temperature between 0.8 and 1.5 °C can be observed on all the profiles between river kilometers 620 and 650 (Fig. 4b). A local temperature minimum is observed on every profile at river kilometer 645, close to La Chapelle-Saint-Mesmin. The temperature increased again from river kilometers 660 to 680 and then remained constant or decreased once more after river

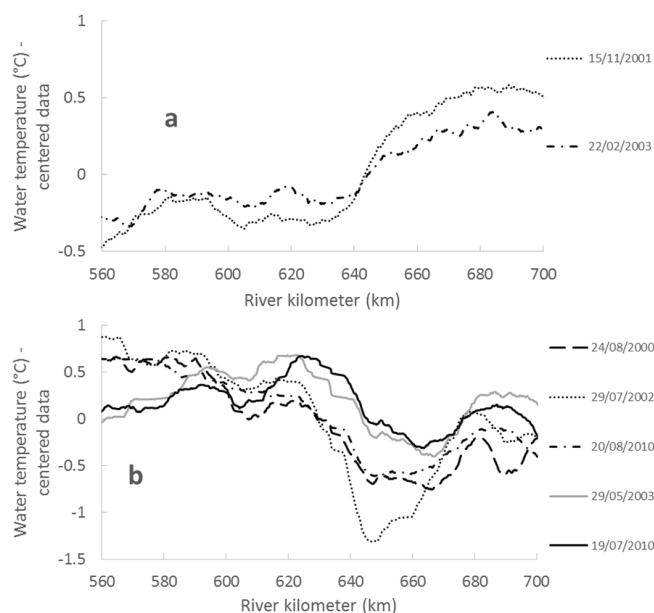


Figure 4. (a) Loire temperature profiles in winter extracted from the TIR images. (b) Loire temperature profiles in summer extracted from the TIR images. For each profile data were centered.

kilometer 680. However, the temperature profiles differ between river kilometers 560 and 620, since the water temperature either increased (29 May 2003 and 19 July 2010; Fig. 4b) or decreased (24 August 2000, 29 July 2002 and 20 August 2010; Fig. 4b). Another difference appears between river kilometers 650 and 660, with either a temperature drop (29 May 2003 and 19 July 2010) or a temperature rise (29 July 2002). Then, from river kilometers 680 to 700, the temperature dropped downstream of river kilometer 690 (29 May 2003, 19 July 2010 and 20 August 2010), or upstream of river kilometer 690 (24 August 2000 and 29 July 2002), and then was followed by a rise in the temperature. In winter the temperature increased sharply by around 0.5 °C between river kilometers 630 and 650 (Fig. 4a).

Sharp temperature changes in the longitudinal profile need to be compared with the uncertainty and not with the accuracy. The sharpest temperature changes observed on the longitudinal profiles were between 0.04 and 0.1 °C km⁻¹ (mean of 0.074 °C km⁻¹). The most marked temperature changes are therefore at least 1 order of magnitude higher than those expected from the uncertainty (0.0072 °C km⁻¹). They are therefore likely to be meaningful.

4.3 Groundwater discharge estimation

The groundwater discharge was estimated at seven dates (winter and summer) along the same successive 11 sections of the Loire, using both heat budget and groundwater modeling (Fig. 5a). The variability of the groundwater discharge estimated with the heat budget was much higher than that es-

Table 3. Standard deviation of water temperature (°C) estimated on all the 200 m sections of the Loire River. Standard deviations were calculated at sections with under 20 water pixels and over 20 water pixels.

Standard deviation of water temperature (°C)	Date						
	24 Aug 2000	15 Nov 2001	29 Jul 2002	22 Feb 2003	29 May 2003	19 Jul 2010	20 Aug 2010
River sections under 20 water pixels	0.70	0.56	0.76	0.32	0.45	0.42	0.52
River sections over 20 water pixels	0.50	0.44	0.73	0.26	0.41	0.41	0.42

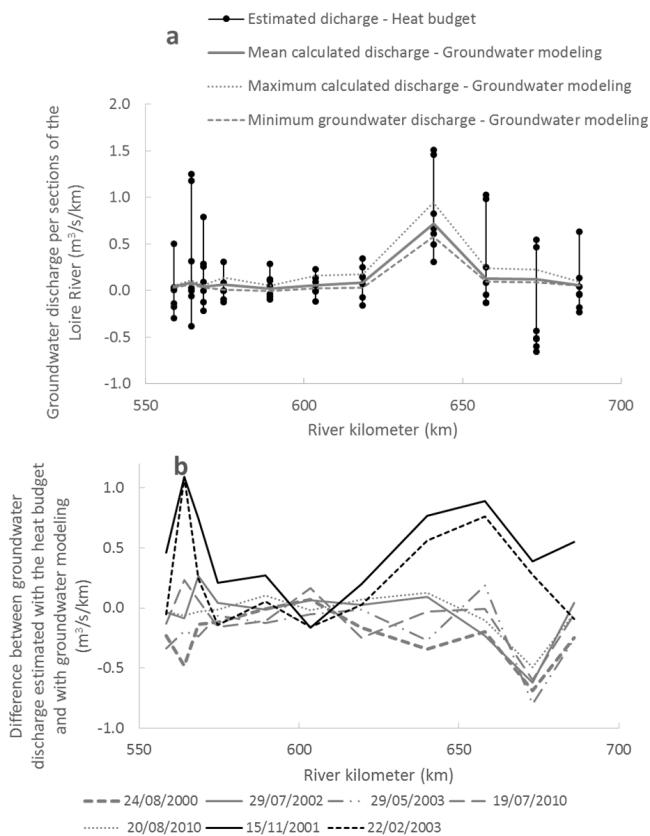


Figure 5. (a) Groundwater discharge per section of the Loire River estimated at the different dates using the heat budget based on the TIR images (black points), and calculated by groundwater modeling (grey line), as a function of the river kilometers. (b) Absolute value of the difference between groundwater discharges estimated by groundwater modeling and the heat budget.

estimated using groundwater modeling (with maximum standard deviations of 0.6 and $0.11 \text{ m}^3 \text{ s}^{-1} \text{ km}^{-1}$, respectively). Nevertheless, the modeled groundwater discharge was always within the interval estimated by the heat budget. Overall, compared to groundwater modeling, the heat budget

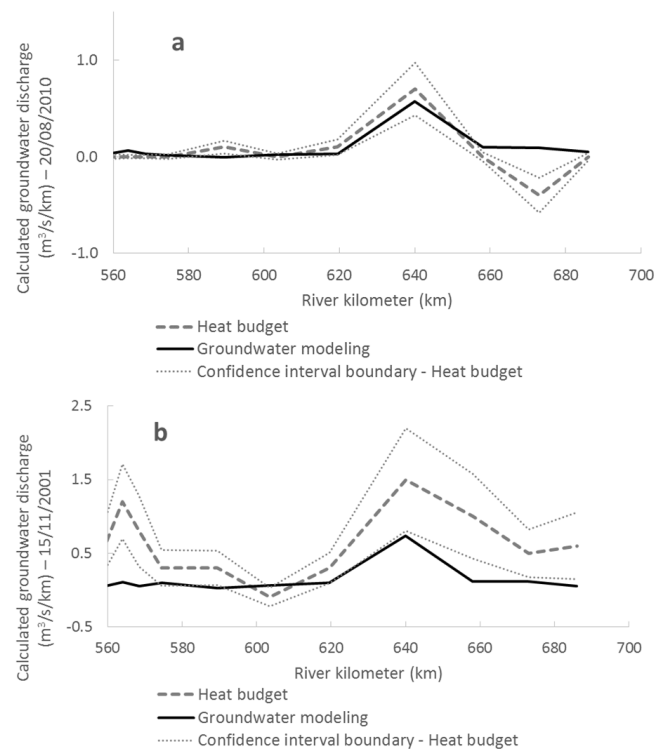


Figure 6. (a) Calculated groundwater discharge along the Loire River on 20 August 2010 using groundwater modeling and the heat budget. (b) Calculated groundwater discharge along the Loire River on 15 November 2001 using groundwater modeling and the heat budget.

tended to overestimate the groundwater discharge between river kilometers 640 and 660 in winter and to underestimate it between river kilometers 660 and 680 in summer (Figs. 5b, 6a, b).

High groundwater discharge rates ($0.31 \text{ m}^3 \text{ s}^{-1} \text{ km}^{-1}$ on average) were calculated with the heat budget method between river kilometers 563 and 565, and they also showed a noticeable increase in the standard deviation ($0.6 \text{ m}^3 \text{ s}^{-1} \text{ km}^{-1}$). However, these high discharge rates and

high standard deviation were not observed using groundwater modeling.

Between river kilometers 570 and 630, the average estimated groundwater discharge using both methods is low (less than 0.3 and $0.1 \text{ m}^3 \text{ s}^{-1} \text{ km}^{-1}$, respectively) and the standard deviation was also low (less than 0.4 and $0.05 \text{ m}^3 \text{ s}^{-1} \text{ km}^{-1}$, respectively).

Further downstream, according to both methods, the groundwater discharge showed a marked peak in the section located between river kilometers 630 and 660. At river kilometer 640, the groundwater discharge estimated with the heat budget was positive at each date (between 0.3 and $1.5 \text{ m}^3 \text{ s}^{-1} \text{ km}^{-1}$) and it also corresponded to where the groundwater discharge was maximal according to groundwater modeling (between 0.6 and $0.9 \text{ m}^3 \text{ s}^{-1} \text{ km}^{-1}$). Both methods showed a high standard deviation of the groundwater discharge (0.4 and $0.1 \text{ m}^3 \text{ s}^{-1} \text{ km}^{-1}$, respectively).

For river kilometers 660 to 680 the results of the two methods were different, with a negative discharge estimated by the heat budget ($-0.24 \text{ m}^3 \text{ s}^{-1} \text{ km}^{-1}$ on average) and a positive discharge calculated by groundwater modeling ($0.12 \text{ m}^3 \text{ s}^{-1} \text{ km}^{-1}$ on average).

Negative flow values were estimated using the heat budget method. Theoretically, the estimated groundwater discharge should not be negative. However, in summer, negative discharge values are computed when water temperature increases but when this increase cannot be explained by atmospheric heat flux. In winter, negative discharge values can also be obtained when water temperature shows a decrease that cannot be explained by atmospheric heat flux.

The absolute uncertainty in the groundwater discharge estimated by the heat budget remained below $0.4 \text{ m}^3 \text{ s}^{-1} \text{ km}^{-1}$ for more than 75 % of the time. Taking into account the uncertainty, in the Loire River section between river kilometers 636 and 645 at all the dates, the estimated groundwater discharge was always above $0.03 \text{ m}^3 \text{ s}^{-1} \text{ km}^{-1}$ and was therefore significant. On this river section, the groundwater discharge estimated with the heat budget was between 2.8 and $13.7 \text{ m}^3 \text{ s}^{-1}$, while that estimated using groundwater modeling varied between 5.2 and $8.6 \text{ m}^3 \text{ s}^{-1}$.

5 Discussion

5.1 Temperature accuracy and uncertainty

There are many factors that can contribute to the accuracy or the uncertainty of the temperature estimation using TIR satellite images. The main factors are the satellite sensors, the atmospheric influence on the transmitted radiation (Kay et al., 2005; Chander et al., 2009; Lamaro et al., 2013), the change in water emissivity with time and along the watercourse, the existing correlation between radiation estimated at neighboring pixels (Handcock et al., 2006) and the thermal stratification of water temperature (Robinson et al., 1984;

Cardenas et al., 2008). The TIR images only measure the temperature of the upper $100 \mu\text{m}$ of the water body (skin layer), which may differ from the temperature of the entire water body (Torgersen et al., 2001).

The average difference between the temperature estimated from the TIR satellite images and the temperature observed in situ was $-0.51 \text{ }^\circ\text{C}$. On average, it is found that temperature estimated using TIR images tends to underestimate real water temperature. However, the opposite has also been regularly observed. Wawrzyniak et al. (2012) found that TIR images overestimated the Rhône River temperature by $+0.5 \text{ }^\circ\text{C}$ on average. Another study was conducted over several watercourses of the Pacific Northwest rivers of the United States (Handcock et al., 2006). A mean temperature difference of $+1.2 \text{ }^\circ\text{C}$ was found when the watercourse width was over 3 image pixels and of $+2.2 \text{ }^\circ\text{C}$ when the width was between 1 and 3 pixels. Mean temperature differences of between $+1$ and $+1.9 \text{ }^\circ\text{C}$ were found in four other Pacific Northwest rivers (Cherkauer et al., 2005).

Negative biases were also found (Barsi et al., 2003). In the case of Lake Tahoe, the temperature estimated with TIR images was on average $1.5\text{--}2.5 \text{ }^\circ\text{C}$ colder than the temperature observed in situ. Similar results were observed on the Wenatchee River in the United States (Cristea and Burges, 2009).

Satellite-based TIR images can therefore lead to either under- or over-estimation of the water temperature. Depending on the time of the year, this difference can be either positive or negative (Lamaro et al., 2013; De Boer, 2014). Findings from this study confirm that water temperature can be either over- or under-estimated using TIR images (Fig. 2). The biggest disparity was observed on 29 July 2002, when the water temperature was maximum ($> 26 \text{ }^\circ\text{C}$) and the flow rate minimum ($60 \text{ m}^3 \text{ s}^{-1}$, i.e., $1.33 \text{ L s}^{-1} \text{ km}^{-2}$). The temperatures from the Loire River were under-estimated at this date. One possible explanation for this would be that high evaporation at this date led to a low temperature of surface water.

The average temperature difference between TIR images and in situ measurements was similar to that observed in previous studies (Handcock et al., 2006; Wawrzyniak et al., 2012), even though in this study non-pure water pixels were included and no atmospheric correction was applied. Temperature estimation using non-pure water pixels from TIR images may therefore be more robust than previously considered. However, this study also shows that differences between temperatures estimated using TIR images and temperatures observed in situ may locally exceed $2 \text{ }^\circ\text{C}$.

The temperature estimated for non-pure water pixels could be influenced by the temperature of the riverbanks. However, tests carried out show that the difference in temperatures estimated using TIR images or measured in situ cannot be explained only by the bias resulting from the use of the non-pure water pixels. Uncertainty resulting from the satel-

lite sensors' low resolution can also play a role, particularly in narrow parts of the Loire.

5.2 Longitudinal temperature profiles and groundwater discharge estimations

TIR images of watercourses have been used in the past to detect groundwater discharge areas and to differentiate them from hyporheic upwelling areas (Burkholder et al., 2007). The surface of the cold water plumes associated with groundwater upwelling has been shown to be correlated with the groundwater discharge rate (Danielescu et al., 2009). However, quantifying groundwater discharge using a river heat budget based on TIR images has only been done once, on a small stream (along a 1.7 km reach, with a flow of $0.01 \text{ m}^3 \text{ s}^{-1}$) and using high-precision aerial images (Loheide and Gorelick, 2006).

This work is new because firstly, groundwater discharge was estimated on a large river, through TIR satellite images, and, secondly, the results were compared with estimations obtained using groundwater modeling. Loheide and Gorelick (2006), on the other hand, compared their findings with groundwater discharge estimated through measurements of the streamflow over successive stream cross sections. This last technique is difficult to use for large rivers and limited section lengths, due to the high uncertainty in flow rate measurements (up to 20 %).

There are several sources of uncertainty in groundwater discharge estimation using the heat budget. First, there is an uncertainty in the estimation of water temperature at the river surface and of the river flow rate. In general in the present study, the resulting uncertainty in groundwater discharge estimate remained below $0.4 \text{ m}^3 \text{ s}^{-1} \text{ km}^{-1}$, which is quite high in case of low groundwater discharge. There are also uncertainties inherent in the heat budget method used as factors such as bed friction, heat conduction through the river bed, or hyporheic exchange are not included. However, for the type of slow flowing river studied, the influence of bed friction is assumed to be low, particularly in summer (Evans et al., 1998). Similarly, heat conduction through the bed usually plays a minor role in the overall river heat budget (Hannah et al., 2008). The effect of heat conduction and hyporheic flows can be confused with the groundwater discharge, which probably leads to a small overestimation of the groundwater discharge. The time for water to travel along the river is not taken into account in the heat budget either. As a result, the river temperature tends to be slightly overestimated due to the influence of the local atmospheric conditions. There are also uncertainties linked to using groundwater modeling to calculate the groundwater discharge. Nevertheless, the modeling of the Loire River flow in Blois, Orléans and Gien over the 1996–2013 period provided good results (Nash criterion of 0.98, correlation of 0.99 and relative bias of $0.01 \text{ m}^3 \text{ s}^{-1}$). Despite all the uncertainties, the groundwater discharge estimated using the heat budget remained within the same order

of magnitude as that calculated using groundwater modeling. It was always below $\pm 1 \text{ m}^3 \text{ s}^{-1} \text{ km}^{-1}$ of the discharge calculated using groundwater modeling. The average groundwater discharge calculated using groundwater modeling was always within the range of variation of the discharge estimated using the river heat budget. The shapes of the average estimated groundwater discharge curve provided by the two methods are also relatively similar (coefficient of determination $r^2 = 0.7$).

On the upstream part of the Loire, i.e., from river kilometers 560 to 635, the groundwater discharge estimated from the heat budget was low (less than $0.3 \text{ m}^3 \text{ s}^{-1} \text{ km}^{-1}$; Fig. 5a), except for some dates around river kilometer 564. This is possibly explained by the fact that the Loire River loses water through the Val d'Orléans karstic system between river kilometers 610 and 625 (Alberic, 2004; Binet et al., 2011). This is also in line with the results from the groundwater modeling. The high standard deviation of the estimated discharge near river kilometer 564 could be explained by both real variations in the discharge rate and the bias resulting from the small length of the corresponding section. Similarly, high groundwater discharge around river kilometer 564 ($0.6 \text{ m}^3 \text{ s}^{-1} \text{ km}^{-1}$) was also found by the BRGM, using the groundwater budget over the successive groundwater catchment areas to calculate the average inter-annual groundwater discharge over the period 1998–2007 (Schomburgk et al., 2012).

A first thermal anomaly appears downstream of river kilometer 620. From river kilometer 636 to river kilometer 645 the groundwater discharge estimated with the heat budget was between 0.3 and $1.5 \text{ m}^3 \text{ s}^{-1} \text{ km}^{-1}$. Taking into account the uncertainties, the groundwater discharge calculated through the heat budget always remained positive between river kilometers 636 and 645. This river section corresponds to a known discharge area of the Beauce aquifer and the Val d'Orléans hydrosystem (Desprez and Martin, 1976; Gonzalez, 1991; Binet et al., 2011), which is also identified by groundwater modeling (calculated discharge was between 0.6 and $0.9 \text{ m}^3 \text{ s}^{-1} \text{ km}^{-1}$). Schomburgk et al. (2012) calculated a slightly lower but still significant groundwater discharge of $0.5 \text{ m}^3 \text{ s}^{-1} \text{ km}^{-1}$. It is interesting to note that along the Loire River, the maximum estimated exchange rates occurred at times when the river flow decreased over two consecutive days, while the lowest exchange rate was estimated when the flow increased (Fig. 7). The maximum groundwater discharge was also estimated in winter ($13.5 \text{ m}^3 \text{ s}^{-1}$ compared to $5.3 \text{ m}^3 \text{ s}^{-1}$ in summer), when the groundwater level was at its highest. This is in line with the results from the groundwater modeling, which show an average discharge of $7.6 \text{ m}^3 \text{ s}^{-1}$ in winter and $6 \text{ m}^3 \text{ s}^{-1}$ in summer. It is known that temporal changes in river water levels can lead to large modifications in exchange rates and directions (Sophocleous, 2002). During a rise in the water level, water can flow into the lateral aquifer, while the opposite is true during low flow rates. Thus, the variation in estimated exchange rates is

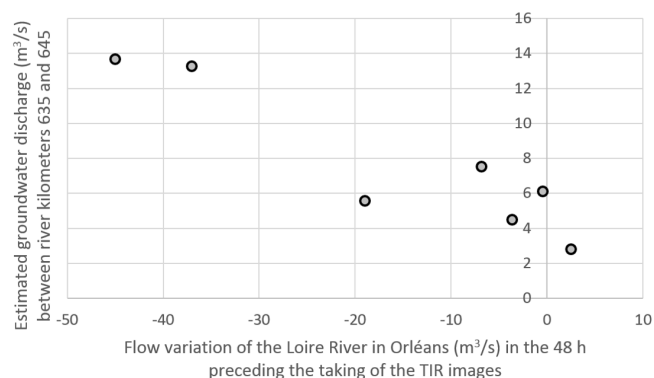


Figure 7. Groundwater discharge rate as a function of the variation in river flow in the 48 h before the TIR image was taken.

likely to have a physical basis. An exchange rate of $11.5\text{--}12.5\text{ m}^3\text{ s}^{-1}$ was calculated at La Chapelle-Saint-Mesmin (river kilometer 642) using geo-chemical tracers during the summer of 1986 (Gonzalez, 1991). This was higher than the maximum groundwater discharge estimated in the summer using the heat budget ($7.5\text{ m}^3\text{ s}^{-1}$). Therefore, the high discharge rates estimated using the heat budget are plausible. The TIR satellite images enable the main groundwater discharge area to be located precisely, along the right bank of the Loire River and 2 to 3 km upstream of the confluence with the Loiret (Fig. 8).

On the downstream part of the Loire River, between river kilometers 650 and 680, both heat budget and groundwater modeling estimations showed a decrease in groundwater discharge. Over the last 20 km downstream, the heat budget would suggest a slight increase in groundwater discharge, in line with the findings from Schomburgk et al. (2012). On the other hand, groundwater modeling predicts a slight decrease in groundwater discharge.

The change in the groundwater discharge rate over time could explain why the river temperature either increased or decreased between river kilometers 645 and 665, or between river kilometers 570 and 620. However, atmospheric factors are also likely to play a role, even though the atmospheric data available do not offer a satisfactory explanation for this phenomenon. The influence of warm water discharged from the nuclear power plant on the longitudinal temperature profile was not noticeable either, as no sudden temperature rise was observed at the locations of the nuclear plants. In the case of Saint-Laurent-des-Eaux, discharged warm water may nevertheless contribute to a certain extent to the overall temperature rise observed between river kilometers 670 and 680 (Fig. 4a, b); however, the temperature rise began upstream of the power plant.

Similarly, no sudden temperature variations could be explained by weirs across the river course or changes in the river slope (less than $0.1\text{ }^\circ\text{C}$ change between a kilometer up- or down-stream of the structure), although abrupt tempera-

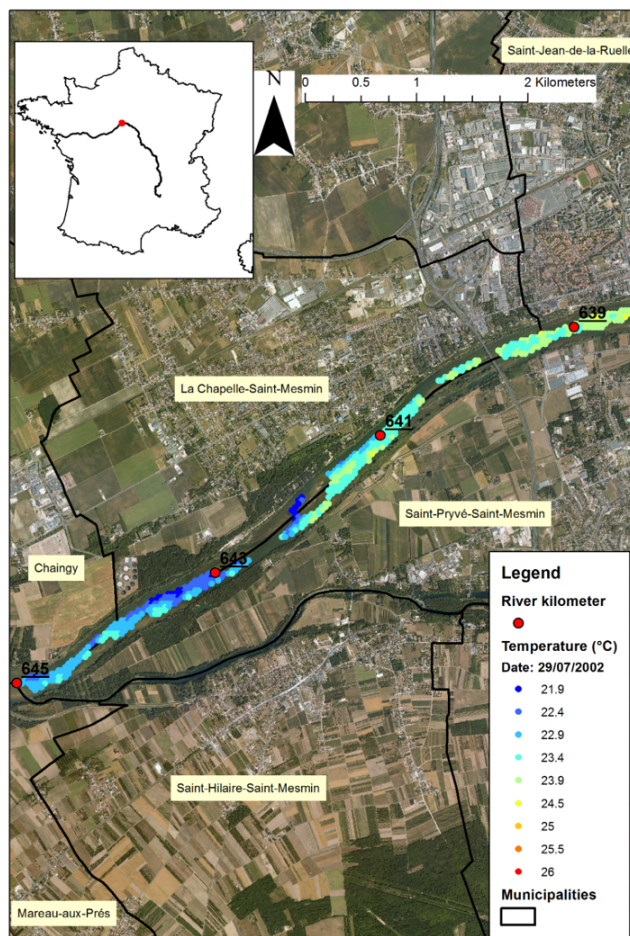


Figure 8. Temperatures measured in the Loire River in the vicinity of La Chapelle-Saint-Mesmin on 29 July 2002. Groundwater discharge is visible along the right bank (northern side) of the Loire River as a cold patch between river kilometers 642 and 644.

ture changes near weirs have been observed on the Ain River in France (Wawrzyniak, 2012) based on airborne TIR images. This could be explained by the small reservoir capacity of the Loire River upstream of the weirs (Casado et al., 2013) and also by the low spatial resolution of the TIR satellite images. The Landsat images were taken around 12:30 LT and thermal stratification could be expected to be greater later in the day.

6 Conclusion

Temperatures of the middle Loire River were estimated using thermal infrared (TIR) Landsat images. Although no atmospheric correction was implemented and non-pure water pixels were taken into account, temperature differences from in situ observations and TIR-image based estimations remain within the interval defined in previous studies (i.e., 75 % of these differences being in the $\pm 1\text{ }^\circ\text{C}$ interval). Therefore, this

study shows that river temperature may be studied from TIR satellite images even when the river width falls below the 3-pixel width threshold (i.e., < 180 m). However, the river temperature can be seriously underestimated at low flow rates and high water temperatures (differences of over 2 °C).

We demonstrate that groundwater discharge to a large river can be estimated using satellite images. The groundwater discharge was estimated along the Loire River using both the heat budget based on the longitudinal temperature profiles established from the TIR images, and a groundwater model. The variations of the groundwater discharge rate along the Loire River were similar with both methods. The main discharge area of the Beauce aquifer into the Loire River is located between river kilometers 636 and 645 (close to La Chapelle-Saint-Mesmin).

According to the TIR images, the average groundwater discharge between river kilometers 636 and 645 appears to be higher in winter than in summer (13.5 and 5.3 m³ s⁻¹, respectively). This is in line with the results from the groundwater modeling, which show an average discharge of 7.6 m³ s⁻¹ in winter and 6 m³ s⁻¹ in summer. The groundwater discharge was also higher when the river flow decreased over two consecutive days. Our TIR images highlight that instantaneous groundwater discharge can vary considerably over time. Therefore, average discharge is not sufficient to predict the observed changes in water temperature along the river course.

To assess the consistency and robustness of these results, further studies could be conducted using more sophisticated modeling of both the groundwater discharge and stream temperature.

Acknowledgements. This work was part of the scientific program “Control factors of river temperature at regional scale in the Loire catchment” funded by European funds for regional development, Etablissement Public Loire and the Loire River basin authority (Agence de l’Eau Loire Bretagne). The calculation of groundwater fluxes using groundwater budget was also funded by Electricité De France (EDF) and monitored by Mohamed Krimissa from EDF.

We would like to thank Alain Poirel from EDF for the hourly Loire River temperature measurements on the days images were taken. We would also like to thank Météo France for the information from the SAFRAN database. Finally, we are very grateful to the water assessment and evaluation team of the BRGM water department, particularly Alexandre Brugeron, for their help in characterizing groundwater catchment areas and groundwater fluxes.

Edited by: M. Gooseff

References

- Alberic, P.: River backflooding into a karst resurgence (Loiret, France), *J. Hydrol.*, 286, 194–202, 2004.
- Alberic, P. and Lepiller, M.: Oxydation de la matière organique dans un système hydrologique karstique alimenté par des pertes fluviales (Loiret, France), *Water Resour.*, 32, 2051–2064, 1998.
- Barsi, J. A., Barker, J. L., and Schott, J. R.: An atmospheric correction parameter calculator for a single thermal band earth-sensing instrument, in: *Geoscience and Remote Sensing Symposium, IGARSS’03, Proceedings, IEEE International*, 21–25 July, Toulouse, France, 3014–3016, 2003.
- Belknap, W. and Naiman, R. J.: A GIS and TIR procedure to detect and map wall-base channels in Western Washington, *J. Environ. Manage.*, 52, 147–160, 1998.
- Binet, S., Auterives, C., and Charlier, J. B.: Construction d’un modèle hydrogéologique d’été sur le val d’Orléans, rapport final, ICERE, Orléans, France, 2011.
- Boyd, M. and Kasper, B.: *Analytical Methods for Dynamic Open Channel Heat and Mass Transfer: Methodology for Heat Source Model Version 7.0*, Watershed Sciences Inc., Portland, Oregon, USA, 2003.
- Burkholder, B. K., Grant, G. E., Haggerty, R., Khangaonkar, T., and Wampler, P. J.: Influence of hyporheic flow and geomorphology on temperature of a large, gravel bed river, Clackamas River, Oregon, USA, *Hydrol. Process.*, 22, 941–953, 2007.
- Bustillo, V., Moatar, F., Ducharme, A., Thiery, D., and Poirel, A.: A multimodel comparison for assessing water temperatures under changing climate conditions via the equilibrium temperature concept: case study of the Middle Loire River, France, *Hydrol. Process.*, 28, 1507–1524, 2014.
- Caissie, D.: The thermal regime of rivers: a review, *Freshwater Biol.*, 51, 1389–1406, 2006.
- Cardenas, B., Harvey, J. W., Packman, A. I., and Scott, D. T.: Ground-based thermography of fluvial systems at low and high discharge reveals potential complex thermal heterogeneity driven by flow variation and bio-roughness, *Hydrol. Process.*, 22, 980–986, 2008.
- Casado, A., Hannah, D. M., Peiry, J. L., and Campo, A. M.: Influence of dam-induced hydrological regulation on summer water temperature: Sauce Grande River, Argentina, *Ecology*, 6, 523–535, 2013.
- Chander, G., Markham, B. L., and Helder, D. L.: Summary of current radiometric calibration coefficients for Landsat MSS, TM, ETM+ and EO-1 ALI sensors, *Remote Sens. Environ.*, 113, 893–903, 2009.
- Chapra, S. C.: *Surface Water-Quality Modeling*, Civil Engineering Series, McGraw-Hill International editions, Singapore, 1997.
- Cherkauer, K. A., Burges, S. J., Handcock, R. N., Kay, J. E., Kampf, S. K., and Gillepsie, A. R.: Assessing satellite based and aircraft based thermal infrared remote sensing for monitoring pacific northwest river temperature, *J. Am. Water Resour. As.*, 41, 1149–1159, 2005.
- Chow, V. T.: *Open Channel Hydraulics*, McGraw Hill Company Inc., New York, 1959.
- Cristea, N. C. and Burges, S. J.: Use of thermal infrared imagery to complement monitoring and modeling of spatial stream temperatures, *J. Hydrol. Eng.*, 14, 1080–1090, 2009.
- Danielescu, S., MacQuarrie, K. T. B., and Faux, N. R.: The integration of thermal infrared imaging, discharge measurements

- and numerical simulation to quantify the relative contributions of freshwater inflows to small estuaries in Atlantic Canada, *Hydrol. Process.*, 23, 2847–2859, 2009.
- De Boer, T.: Assessing the accuracy of water temperature determination and monitoring of inland surface waters using Landsat 7 ETM+ thermal infrared images, MS thesis, Delft University, Delft, the Netherlands, 2014.
- Desprez, N. and Martin, C.: Inventaire des points d'eau – piézométrie et bathymétrie des alluvions du lit majeur de la Loire entre Saint-Hilaire Saint-Mesmin et Saint-Laurent des Eaux, Rep. 76 SGN 461 BDP, BRGM, Orléans, France, 1976.
- Etchevers, P., Golaz, C., and Habets, F.: Simulation of the water budget and the river flows of the Rhone basin from 1981 to 1994, *J. Hydrol.*, 244, 60–85, 2001.
- Evans, E. C., McGregor, G. R., and Petts, G. E.: River energy budgets with special reference to river bed processes, *Hydrol. Process.*, 12, 575–595, 1998.
- Flipo, N., Monteil, C., Poulin, M., De Fouquet, C., and Krimissa, M.: Hybrid fitting of a hydrosystem model: long-term insight into the Beauce aquifer functioning (France), *Water Resour. Res.*, 48, W05509, doi:10.1029/2011WR011092, 2012.
- Fullerton, A. H., Torgersen, C. E., Lawler, J. L., Faux, R. N., Steel, E. A., Beechie, T. J., Ebersole, J. L., and Leibowitz, S. G.: Rethinking the longitudinal stream temperature paradigm: region-wide comparison of thermal infrared imagery reveals unexpected complexity of river temperature, *Hydrol. Process.*, doi:10.1002/hyp.10506, online first, 2015.
- Gonzalez, R.: Étude de l'organisation et évaluation des échanges entre la Loire moyenne et l'aquifère des calcaires de Beauce, PhD thesis, Université d'Orléans, Orléans, France, 1991.
- Gutierrez, A. and Binet, S.: La Loire souterraine: circulations karstiques dans le val d'Orléans, *Géosciences*, 12, 42–53, 2010.
- Habets, F., Etchevers, P., Golaz, C., Leblois, E., Ledoux, E., Martin, E., Noilhan, J., and Otlé, C.: Simulation of the water budget and the river flows of the Rhône basin, *J. Geophys. Res.*, 104, 31145–31172, 1999.
- Handcock, R. N., Gillepsie, A. R., Cherkauer, K. A., Kay, J. E., Burges, S. J., and Kampf, S. K.: Accuracy and uncertainty of thermal-infrared remote sensing of stream temperatures at multiple spatial scales, *Remote Sens. Environ.*, 100, 427–440, 2006.
- Handcock, R. N., Torgersen, C. E., Cherkauer, K. A., Gillepsie, A. R., Tockner, K., Faux, R. N., and Tan, J.: Thermal infrared sensing of water temperature in riverine landscapes, in: *Fluvial Remote Sensing for Science and Management*, 1st edn., edited by: Carbonneau, P. E. and Piégay, H., John Wiley & Sons, Ltd., Chichester, UK, 2012.
- Hannah, D. M., Malcolm, I. A., Soulsby, C., and Youngson, A. F.: Heat exchanges and temperatures within a salmon spawning stream in the Cairngorms, Scotland: seasonal and sub-seasonal dynamics, *River Res. Appl.*, 20, 635–652, 2004.
- Hannah, D. M., Malcolm, I. A., Soulsby, C., and Youngson, A. F.: A comparison of forest and moorland stream microclimate, heat exchanges and thermal dynamics, *Hydrol. Process.*, 22, 919–940, 2008.
- Kay, J. E., Kampf, S. K., Handcock, R. N., Cherkauer, K. A., Gillepsie, A. R., and Burges, S. J.: Accuracy of lake and stream temperatures estimated from thermal infrared images, *J. Am. Water Resour. As.*, 41, 1161–1175, 2005.
- Lamaro, A. A., Marinelarena, A., Torrusio, S. E., and Sala, S. E.: Water surface temperature estimation from Landsat 7 ETM+ thermal infrared data using the generalized single-channel method: case study of Embalse del Rio Tercero (Cordoba, Argentina), *Adv. Space Res.*, 51, 492–500, 2013.
- Latapie, A., Camenen, B., Rodrigues, S., Paquier, A., Bouchard, J. P., and Moatar, F.: Assessing channel response of a long river influenced by human disturbance, *Catena*, 121, 1–12, 2014.
- Ledoux, E., Gomez, E., Monget, J., Viavattene, C., Viennot, P., Ducharne, A., Benoit, M., Mignolet, C., Schott, C., and Mary, B.: Agriculture and groundwater nitrate contamination on the Seine basin. The STICS-MODCOU modelling chain, *Sci. Total Environ.*, 375, 33–47, 2007.
- Loheide, S. P. and Gorelick, S. M.: Quantifying stream-aquifer interactions through the analysis of remotely sensed thermographic profiles and in-situ temperature histories, *Environ. Sci. Technol.*, 40, 3336–3341, 2006.
- Mallast, U., Gloaguen, R., Friesen, J., Rödiger, T., Geyer, S., Merz, R., and Siebert, C.: How to identify groundwater-caused thermal anomalies in lakes based on multi-temporal satellite data in semi-arid regions, *Hydrol. Earth Syst. Sci.*, 18, 2773–2787, doi:10.5194/hess-18-2773-2014, 2014.
- Moatar, F. and Gailhard, J.: Water temperature behaviour in the river Loire since 1976 and 1881, *Surf. Geosci.*, 338, 319–328, 2006.
- Monk, W. A., Wilbur, N. M., Curry, R. A., Gagnon, R., and Faux, R. N.: Linking landscape variables to cold water refugia in rivers, *J. Environ. Manage.*, 1, 170–176, 2013.
- Monteil, C.: Estimation de la contribution des principaux aquifères du bassin versant de la Loire au fonctionnement hydrologique du fleuve à l'étiage, PhD thesis, Mines Paris Tech, Paris, France, 2011.
- Pryet, A., Labarthe, B., Saleh, F., Akopian, M., and Flipo, N.: Reporting of stream-aquifer flow distribution at the regional scale with a distributed process-based model, *Water Resour. Manag.*, 29, 139–159, 2015.
- Quintana-Segui, P., Moigne, P. L., Durand, Y., Martin, E., Habets, F., Baillon, M., Canellas, C., Franchisteguy, L., and Morel, S.: Analysis of near surface atmospheric variables: validation of the SAFRAN analysis over France, *J. Appl. Meteorol. Clim.*, 47, 92–107, 2008.
- Robinson, I. S., Wells, N. C., and Charnock, H.: The sea surface thermal boundary layer and its relevance to the measurements of sea surface temperature by airborne and spaceborne radiometers, *Int. J. Remote Sens.*, 5, 19–45, 1984.
- Rushton, K.: Representation in regional models of saturated river-aquifer interaction for gaining-losing rivers, *J. Hydrology*, 334, 262–281, 2007.
- Saleh, F., Flipo, N., Habets, F., Ducharne, A., Oudin, L., Viennot, P., and Ledoux, E.: Modeling the impact of in-stream water level fluctuations on stream-aquifer interactions at the regional scale, *J. Hydrol.*, 400, 490–500, 2011.
- Salencon, M. J. and Thébault, J. M.: Modélisation d'écosystème lacustre, Masson, Paris, France, 1997.
- Schomburgk, S., Brugeron, A., Winkel, A., Ruppert, N., Salquebre, D., and Martin, J. C.: Contribution des principaux aquifères au fonctionnement hydrologique de la Loire en région Centre – Caractérisation et bilans par bassins versants souterrains, BRGM, Orléans, France, Rep. BRGM/RP 60381-FR, 2012.

- Smikrud, K. M., Prakash, A., and Nichols, J. V.: Decision-based fusion for improved fluvial landscape classification using digital aerial photographs and forward looking infrared images, *Photogramm. Eng. Rem. S.*, 74, 903–911, 2008.
- Sophocleous, M.: Interactions between groundwater and surface water: the state of science, *Hydrogeol. J.*, 10, 52–67, 2002.
- Tonolla, D., Acuna, V., Uehlinger, U., Frank, T., and Tockner, K.: Thermal heterogeneity in river floodplains, *Ecosystems*, 13, 727–740, 2010.
- Torgersen, C. E., Price, D. M., Li, H. W., and McIntosh, B. A.: Multiscale thermal refugia and stream habitat associations of Chinook salmon in northeastern Oregon, *Ecol. Appl.*, 9, 301–319, 1999.
- Torgersen, C. E., Faux, R. N., McIntosh, B. A., Poage, N. J., and Norton, D. J.: Airborne thermal remote sensing for water temperature assessment in rivers and streams, *Remote Sens. Environ.*, 76, 386–398, 2001.
- USGS (US Geological Survey): Landsat-A Global Land-Imaging Mission, US Geological Survey Fact sheet, Sioux Falls, Dakota, USA, 4 pp., 2012, revised: 30 May 2013.
- Wang, L. T., McKenna, T. E., and DeLiberty, T. L.: Locating ground-water discharge areas in Rehoboth and Indian River bays and Indian River, Delaware, using Landsat 7 imagery, Report of investigation no. 74, Delaware Geological Survey, Newark, DE, USA, 2008.
- Ward, J. V.: *Aquatic Insect Ecology, Part I, Biology and Habitat*, Wiley & Son, New York, USA, 1992.
- Wawrzyniak, V.: Etude multi-échelle de la température de surface des cours d'eau par imagerie infrarouge thermique: exemples dans le bassin du Rhône, PhD thesis, Université Jean-Moulin, Lyon, France, 2012.
- Wawrzyniak, V., Piégay, H., and Poirel, A.: Longitudinal and temporal thermal patterns of the French Rhône River using Landsat ETM+ thermal infrared (TIR) images, *Aquat. Sci.*, 74, 405–414, 2012.
- Wawrzyniak, V., Piégay, H., Allemand, P., Vaudor, L., and Grandjean, P.: Prediction of water temperature heterogeneity of braided rivers using very high resolution thermal infrared (TIR) images, *Int. J. Remote Sens.*, 34, 4812–4831, 2013.
- Webb, B. W. and Zhang, Y.: Spatial and seasonal variability in the components of the river heat budget, *Hydrol. Process.*, 11, 79–101, 1997.
- Webb, B. W. and Zhang, Y.: Water temperatures and heat budgets in Dorset chalk water courses, *Hydrol. Process.*, 13, 309–321, 1999.